Simulation of Flexible-Link Manipulators With Inertial and Geometric Nonlinearities

Chris Damaren
Assistant Professor,
Department of Engineering,
Royal Roads Military College,
FMO Victoria, British Columbia,
V0S 1B0

Inna Sharf
Assistant Professor,
Department of Mechanical Engineering,
University of Victoria,
Victoria, British Columbia, Canada
V8W 3P6

Several important issues relevant to modeling of flexible-link robotic manipulators are addressed in this paper. First, we examine the question of which inertial nonlinearities should be included in the equations of motion for purposes of simulation. A complete model incorporating all inertial terms that couple rigid-body and elastic motions is presented along with a rational scheme for classifying them. Second, the issue of geometric nonlinearities is discussed. These are terms whose origin is the geometrically nonlinear theory of elasticity, as well as the terms arising from the interbody coupling due to the elastic deformation at the link tip. Accordingly, a general way of incorporating the well-known geometric stiffening effect is presented along with several schemes for treating the elastic kinematics at the joint interconnections. In addition, the question of basis function selection for spatial discretization of the elastic displacements is also addressed. The finite element method and an eigenfunction expansion techniques are presented and compared. All issues are examined numerically in the context of a simple beam example and the Space Shuttle Remote Manipulator System. Unlike a single-link system, the results for the latter show that all terms are required for accurate simulation of faster maneuvers. Hence, the conclusions of the paper are contrary to some of the previous findings on the validity of various models for dynamics simulation of flexible-body systems.

1 Introduction

Dynamics simulation of robotic manipulators with flexible links has received a great deal of attention in the last several years. This problem, although it has gained importance in industrial robotics, is particularly relevant to space applications of manipulators. Space robotic systems are made up of lightweight, large in size members and, therefore, exhibit significant structural flexibility. Moreover, ground-based experiments with these systems are difficult because of the gravitation field, and are prohibitively expensive to carry out in space. Hence, the capability to simulate the dynamics of space manipulators is essential for design, development of control strategies, as well as, real-time applications such as animation.

A number of formulations and solution algorithms have been proposed for dynamical simulation of flexible-link robots. A literature review on the topic has been published by Gaultier and Cleghorn [1]. The more recent works include Bae and Haug [2], Serna and Bayo [3], Naganathon and Soni [4], Wehage and Shabana [5], Hughes and Sincarsin [6], Nagarajan and Turcic [7], and D'Eleuterio [8]. These vary in the approach taken to develop the motion equations, the techniques used to model the elasticity of the links, the assumptions made with regards to the coupling of rigid-body motion and elastic deformations, and, correspondingly, the complexity of the dynamics models. Despite their differences, however, most of the existing formulations are based on the classical or linear theory of elasticity. This implies that the governing equations of motion do not contain terms which are nonlinear in the elastic variables.

In the last few years, a number of researchers have observed that the use of classical theory to describe the motion of elastic bodies comprising multibody systems yields a set of dynamics equations which inherently lack what is usually referred to as the geometric stiffening term. Kane et al. [9] were among the first to point out this deficiency of traditional multibody dynamics formulations and the consequent inade-

Contributed by the Dynamic Systems and Control Division for publication in the JOURNAL OF DYNAMIC SYSTEMS, MEASUREMENT, AND CONTROL. Manuscript received by the DSCD April 29, 1993; revised manuscript received February 11, 1994. Associate Technical Editor: A. G. Ulsoy.

quacy of the existing simulation software. They considered a flexible beam attached to a base which undergoes general prescribed motion. Kane et al. [9] developed a set of equations that describe the deformation of the beam by employing a nonlinear expression for the stretch coordinate. They also incorporate in their formulation some of the "specialized" beam properties, such as rotary inertia and shear deformation, nonuniform geometric and material properties, and warping. Simo and Vu-Quoc [10] demonstrated analytically the failure of linear beam theory to predict the centrifugal stiffening effect and proposed a formulation based on the fully nonlinear or geometrically exact theory for beams and plates. In addition to properly accounting for stiffening, their procedure allows one to develop the motion equations of the system in the inertial, rather than the traditionally employed floating or shadow reference frame [11]. Interestingly, the geometric stiffening effect was included long ago in the treatment of planar rotating beams by Likins et al. [12], Vigneron [13] and Kaza and Kvaternik [14]. Since then, a number of problems dealing with multibody systems in a variety of applications have been addressed (see for example, Lips and Modi [15], Hughes and Fung [16], Simo and Vu-Quoc [17], Banerjee and Lemak [18], and Walrapp [19]. All of these works incorporate geometric stiffening in the governing equations, although via different routes.

In the context of flexible-link manipulator simulation, the geometric stiffening effects have been considered by Padilla and von Flotow [20], Ider and Amirouche [21], and van Woerkom [22]. In the former reference, Padilla and von Flotow investigate the effect of three linearization strategies on the form of the motion equations. These researchers justify the inclusion of the geometric stiffening term by arguing that it is linear in the elastic displacements, and hence, is derived with the "consistent" linearization procedure. Ider and Amirouche develop a general set of motion equations applicable to multibody systems with closed loops. However, they as well as Padilla and von Flotow, present simulation results for a flexible beam and a two-link planar manipulator only. Van Woerkom discusses four techniques that can be used to account for the stiffening effect in the dynamics models and presents numerical results for the eigenfrequencies of a single link with tip mass.

The main objective and contribution of this paper are to identify the different types and orders of nonlinearities present in the dynamics equations of a flexible body. These equations are written in the floating frame. They are derived by employing an exact description of the velocity distribution in the elastic body as well as exact nonlinear strain-displacement equations. Due to the latter, they include the geometric stiffening terms. The resulting dynamics equations can be considered "exact" in the sense that they contain all of the nonlinear terms obtained from the two aforementioned relations. In practice, however, this model becomes inexact through the assumed displacement and rotation fields. By contrast, successive approximations to the geometrically exact model of Simo and Vu-Quoc [10] can be constructed by approximating the nonlinear strain measures.

We begin our classification by subdividing the nonlinear terms into three basic categories. Those in the first category will be referred to as the inertial nonlinearities, since they originate from the nonlinear term in the exact expression for the velocity distribution. Accordingly, they appear in the motion equations through the expression for kinetic energy if one employes Lagrange's or Hamiltonian formulations, or through the inertial forces if one uses a vectorial formulation, such as Newton-Euler. As pointed out by Simo and Vu-Quoc [11], these nonlinearities appear in the dynamics equations when the motion of a flexible body is referred to the floating, not the inertial frame. We refer to these nonlinearities as inertial since indeed they can only be present when a flexible body undergoes rigid-body motion.

The inertial nonlinear terms exist independently of the second category of nonlinearities, which are those that arise from employment of nonlinear theory of elasticity to describe the kinematics of elastic deformation. Following Shabana [23], we refer to these as geometric elastic nonlinearities since they appear in the dynamics equations in the form of nonlinear elastic forces. These are derived from the strain energy of an elastic body which in turn is determined with the nonlinear strain-displacement relations.

The third group of nonlinearities, also geometric in nature, arises when considering the kinematical constraints governing neighbouring links. They can be attributed to the elastic displacement and rotation at the "tip" of one body upon interconnection with its neighbor. The rotation, in particular, can be subjected to a number of approximations which simplify the treatment. Part of our task is to ascertain the veracity of these approximations, which are ubiquitous in the current literature.

In each of the above categories, we identify the form of the various nonlinear terms and further classify them according to their order. The inertial nonlinear terms can also be described as "hybrid" or rigid-elastic terms since, as was alluded to earlier, they represent the coupling between the rigid-body and elastic motions. For instance, one can identify terms of $O(\|\dot{\mathbf{q}}_{n,e}\|\,\|\mathbf{v}_n\|)$ which represent the dynamical effects due to products of elastic rates $\dot{\mathbf{q}}_{n,e}$ and rigid velocities $\mathbf{v}_n$. In the previous work [24], the authors defined three types of hybrid terms and demonstrated their effects on the simulated motion of the Space Shuttle Remote Manipulator System. Motivated by these results, we now subdivide the inertial terms into two classes only. The first "order" of nonlinear terms is defined to include the inertial forcing terms of $O(\|\dot{\mathbf{q}}_{n,e}\|\,\|\mathbf{v}_n\|)$, $O(\|\dot{\mathbf{q}}_{n,e}\|\,\|\mathbf{q}_{n,e}\|\,\|\mathbf{v}_n\|)$ and $O(\|\mathbf{q}_{n,e}\|\,\|\mathbf{v}_n\|^2)$. These hybrid terms contribute to the forcing component of the differential equations. The second group of nonlinear inertial terms includes all those remaining. These are the $O(\|\mathbf{q}_{n,e}\|^2)$ terms which augment first and second moments of inertia of the body to account for its deformation during motion.

The classification of the geometric nonlinear terms is more straightforward since their nonlinearity is characterized strictly by the order of elastic displacements. Thus, we distinguish first and second order of geometric elastic nonlinearities, which correspond to the terms in the motion equations of $O(\|\mathbf{q}_{n,e}\|^2)$ and $O(\|\mathbf{q}_{n,e}\|^3)$. The geometric interbody nonlinearities are categorized according to the approximation adopted for the interjoint position vector and interbody elastic rotation.

The second goal of the paper is to illustrate the effects of the various types of nonlinearities for a general robotic

system. To this end, we propose four dynamics models, each specified by the type and order of nonlinear terms included in the equations. Thus, ruthlessly linearized, inconsistently linearized, consistently linearized, and exact models are defined where the first one represents the dynamics equations, which do not contain any nonlinear terms, and the last one corresponds to the "exact" equations. Since the subject of geometric stiffening has been discussed extensively in the context of a single flexible-beam, we first present the numerical results obtained with the different models for a well-known spin-up problem. This is done primarily with the purpose of placing the models in the framework of existing formulations, as well as verifying our simulation results.

As an example of a three-dimensional, six-degree-of-freedom robotic manipulator with elastic members, we choose a 6-link manipulator modeled after the shuttle arm. In order to compare the applicability of the four models introduced earlier, the results are presented for two classes of maneuvers which illustrate responses to smooth and step inputs. In each class, we further consider two types of maneuvers which yield similar trajectories, but are executed at different speeds. This selection allows us to highlight the differences between the models and, consequently, the relative importance of the nonlinear terms for various maneuver speeds. The goodness of the models is verified by monitoring the energy drift for the shuttle manipulator (plus payload) system.

In addition to presenting a series of numerical solutions obtained with different models, we also demonstrate the use of two discretization strategies to describe the elastic deformation in the links. These are the finite-element method and the normal modes method. Both procedures are based on the Euler-Bernoulli beam theory of bending and the engineering theory of torsion. Mayo and Dominguez [25] have also studied these discretization methods in the context of geometrically nonlinear models. They numerically treated a flexible slider-crank mechanism using an existing multibody dynamics software package in conjunction with nonlinear elastic modelling similar to that employed in this work.

2 Classification of Nonlinearities for a Deformable Body

2.1 Equations of Motion for a Single Body. The dynamics equations for an unconstrained deformable body in general motion have been derived previously in a number of publications. Hence, we do not develop them here, but include two key relationships prior to stating the motion equations. These are expressions describing the kinematics of an elastic body and, therefore, are fundamental to any dynamics formulation.

We express the velocity distribution of $\mathcal{B}_n$ as

$$\mathbf{v}_n(\mathbf{r}_n, t) = \mathbf{v}_n(t) - (\mathbf{r}_n + \mathbf{u}_{n,e})^{\times} \boldsymbol{\omega}_n(t) + \dot{\mathbf{u}}_{n,e}(\mathbf{r}_n, t) \qquad (1)$$

where $\mathbf{v}_n$ and $\boldsymbol{\omega}_n$ are the absolute velocity and angular velocity of the inboard articulation point of $\mathcal{B}_n$, O_n, expressed in a floating frame attached to $\mathcal{B}_n$ at O_n; $\mathbf{u}_{n,e}$ is the elastic displacement of the point located at $\mathbf{r}_n$ in the undeformed configuration. The subscript e connotes elastic. The absolute velocities can be collected into a single generalized velocity vector $\nu_n \triangleq \text{col}\{\mathbf{v}_n, \boldsymbol{\omega}_n\}$ which is a 6×1 column matrix. We note that the velocity distribution as given by (1) is exact and contains a nonlinear term $\mathbf{u}_{n,e}^{\times} \boldsymbol{\omega}_n$. It is identical to that adopted in most existing formulations (see, for example, [4], [9], and [26]).

To obtain the discrete dynamics model, the elastic deflection $\mathbf{u}_{n,e}$ is discretized according to

$$\mathbf{u}_{n,e}(\mathbf{r}_n, t) = \sum_{\alpha=1}^{s_n} \boldsymbol{\psi}_{n\alpha}(\mathbf{r}_n) q_{n\alpha}(t) \qquad (2)$$

where we assume that the shape functions $\boldsymbol{\psi}_{n\alpha}$ satisfy cantilevered boundary conditions at $\mathbf{r}_n = 0$; s_n denotes the number of elastic degrees of freedom. We note that in the present formulation the rotation field is not discretized independently of the displacement field, as is done in the formulations of Simo and Vu-Quoc [10, 27] and Cardona and Geradin [28]. This does not effect the general form of the motion equations, nor the inertial terms. As will be noted in Section 2.3.1, the approximation for the rotation field does effect the form of the stiffness term. We also point out that contrary to what has been stated by Kane et al. [9], the expansion (2) for the displacement field does not preclude interdependence between the three components of $\mathbf{u}_{n,e}$, in particular, the "axial" and "transverse" displacements. Therefore, nor does it prohibit modeling the dynamic stiffening of the body during its motion.

With the velocity and elastic displacement distributions (1) and (2) and with the definition $\mathbf{q}_{n,e} \triangleq \text{col}\{q_{n\alpha}\}$, the exact general equations of motion for an elastic body can be written in the form:

$$\begin{aligned} \hat{\mathfrak{M}}_{n,rr}\dot{\nu}_n + \hat{\mathfrak{M}}_{n,re}\ddot{\mathbf{q}}_{n,e} &= \hat{\mathbf{f}}_{nT,r} + \hat{\mathbf{f}}_{nI,r}, \\ \hat{\mathfrak{M}}^{T}_{n,re}\dot{\nu}_n + \mathfrak{M}_{n,ee}\ddot{\mathbf{q}}_{n,e} + \hat{\mathbf{S}}_{n,ee} &= \mathbf{f}_{nT,e} + \hat{\mathbf{f}}_{nI,e} \end{aligned} \qquad (3)$$

Here, $\hat{\mathfrak{M}}_{n,rr}$, $\hat{\mathfrak{M}}_{n,re}$, and $\mathfrak{M}_{n,ee}$ are the mass matrices; $\hat{\mathbf{S}}_{n,ee}$ is the vector of internal (elastic) forces and it represents the stiffness term. We have used the overhat notation to designate the quantities which are dependent on the deformed configuration of the body through elastic coordinates. In the linearized model, the stiffness term is linear in elastic coordinates and all body matrices are constant. The right-hand side of Eq. (3) contains the total generalized forces and the generalized nonlinear inertial forces, rigid and elastic.

As will be shown in the following two sections, the configuration-dependent components of the mass matrices and the hybrid inertial forces result strictly from what we refer to as inertial nonlinearities. By contrast, the nonlinear form of the stiffness term is the result of the geometric nonlinearity or nonlinear kinematics of deformation. In the present formulation, the elastic forces are obtained from the strain energy expression formulated with the nonlinear strain-displacement relations. It is noted that the equations of motion (3) represent a discrete counterpart of the continuous equations developed by Meirovitch [26]. The derivation of equations via the Newton-Euler formulation is detailed in the unpublished manuscript [29], although in it, D'Eleuterio does not provide an explicit form for the stiffness operator.

Before proceeding to the next section where we give a detailed classification of the inertial and geometric nonlinearities, it is worthwhile mentioning that this partition of the nonlinearities in the dynamics equations of an elastic body undergoing general rigid-body motions is not unique. For example, Kane et al. [9] incorporate the nonlinear kinematics

of deformation through their generalized inertia forces. In the approach of Simo and Vu-Quoc [11], the inertial nonlinearities are effectively transferred to the stiffness term by describing the motion with respect to the inertial frame. However, we believe that the classification proposed here reflects the fundamental nature of these nonlinear terms and, moreover, it follows naturally from any procedure for deriving the motion equations that uses (1) and (2) as the basic kinematical description.

2.2 Inertial Nonlinear Terms. The division of inertial nonlinear terms described here is somewhat arbitrary as it is not based on the order of these terms. In fact, such a classification cannot be specified uniquely, since the order of these hybrid terms may be defined with respect to either the order of elastic coordinates and/or their rates and/or rigid velocities. Instead, we delimit the two groups of inertial nonlinearities in accordance with the two inertial components of the motion equations to which they contribute.

The first "order" of nonlinear terms is defined so that it includes the inertial forcing terms of $O(\|\dot{\mathbf{q}}_{n,e}\|\ \|\boldsymbol{\nu}_n\|)$, $O(\|\dot{\mathbf{q}}_{n,e}\|\ \|\mathbf{q}_{n,e}\|\ \|\boldsymbol{\nu}_n\|)$ and $O(\|\mathbf{q}_{n,e}\|\ \|\boldsymbol{\nu}_n\|^2)$. These hybrid terms contribute to the forcing component of the dynamics equations, in particular, $\hat{\mathbf{f}}_{nT,r}$, $\hat{\mathbf{f}}_{nI,r}$, and $\hat{\mathbf{f}}_{nI,e}$. Accordingly, these quantities are defined as follows:

$$\begin{aligned}\hat{\mathbf{f}}_{nT,r} &= \mathbf{f}_{nT,r} + \delta\mathbf{f}_{nT,r}\\ \hat{\mathbf{f}}_{nI,r} &= \mathbf{f}_{nI,r} + \delta\mathbf{f}_{nI,r}\\ \hat{\mathbf{f}}_{nI,e} &= \mathbf{f}_{nI,e} + \delta\mathbf{f}_{nI,e}\end{aligned} \tag{4}$$

where

$$\mathbf{f}_{nT,r} = \begin{bmatrix} \int_{\mathcal{B}_n} \mathbf{f}_n dV_n \\ \int_{\mathcal{B}_n} \mathbf{r}_n^{\times}\mathbf{f}_n dV_n \end{bmatrix}$$

$$\mathbf{f}_{nI,r} = \begin{bmatrix} -m_n\boldsymbol{\omega}_n^{\times}\mathbf{v}_n + \boldsymbol{\omega}_n^{\times}\mathbf{c}_n^{\times}\boldsymbol{\omega}_n \\ -\mathbf{c}_n^{\times}\boldsymbol{\omega}_n^{\times}\mathbf{v}_n - \boldsymbol{\omega}_n^{\times}\mathbf{J}_n\boldsymbol{\omega}_n \end{bmatrix}$$

$$\mathbf{f}_{nI,e} = \text{col}\{-\mathbf{P}_{n\alpha}^T\boldsymbol{\omega}_n^{\times}\mathbf{v}_n - \boldsymbol{\omega}_n^T\boldsymbol{\tau}_{n\alpha}\boldsymbol{\omega}_n\},\ \alpha = 1 \dots s_n \tag{5}$$

and for completeness, we include the definition of the total generalized elastic force:

$$\mathbf{f}_{nT,e} = \text{col}\left\{\int_{\mathcal{B}_n} \boldsymbol{\psi}_{n\alpha}^T\mathbf{f}_n\, dV_n\right\},\ \alpha = 1 \dots s_n \tag{6}$$

Note, that the inertial forces $\mathbf{f}_{nI,r}$ and $\mathbf{f}_{nI,e}$ involve only "rigid-motion" nonlinearities. The first of the modal integrals used in the definition of $\mathbf{f}_{nI,e}$ is given by:

$$\boldsymbol{\tau}_{n\alpha} \triangleq \int_{\mathcal{B}_n} \boldsymbol{\psi}_{n\alpha}^{\times}\mathbf{r}_n^{\times} dm_n \tag{7}$$

The hybrid (δ–) terms in (4) are determined according to:

$$\delta\mathbf{f}_{nT,r} = \begin{bmatrix} 0 \\ \sum_{\alpha=1}^{s_n} \int_{\mathcal{B}_n} \boldsymbol{\psi}_{n\alpha}^{\times}\mathbf{f}_n dV_n q_{n\alpha} \end{bmatrix}$$

$$\delta\mathbf{f}_{nI,r} = \begin{bmatrix} -2\sum_{\alpha=1}^{s_n} \boldsymbol{\omega}_n^{\times}\mathbf{P}_{n\alpha}\dot{q}_{n\alpha} \\ 2\sum_{\alpha=1}^{s_n} \hat{\boldsymbol{\tau}}_{n\alpha}^T\boldsymbol{\omega}_n\dot{q}_{n\alpha} \end{bmatrix}$$

$$\delta\mathbf{f}_{nI,e} = \text{col}\left\{2\sum_{\beta=1}^{s_n} \boldsymbol{\nu}_{n,\beta\alpha}^T\boldsymbol{\omega}_n\dot{q}_{n\beta}\right\},\ \alpha = 1 \dots s_n \tag{8}$$

which requires two additional modal integrals:

$$\begin{aligned}\boldsymbol{\nu}_{n,\alpha\beta} &\triangleq -\int_{\mathcal{B}_n} \boldsymbol{\psi}_{n\alpha}^{\times}\boldsymbol{\psi}_{n\beta}\, dm_n,\\ \boldsymbol{\Upsilon}_{n,\alpha\beta} &\triangleq \int_{\mathcal{B}_n} \boldsymbol{\psi}_{n\alpha}^{\times}\boldsymbol{\psi}_{n\beta}^{\times} dm_n\end{aligned} \tag{9}$$

The second of the above is used in:

$$\hat{\boldsymbol{\tau}}_{n\alpha} \triangleq \boldsymbol{\tau}_{n\alpha} + \sum_{\beta=1}^{s_n} \boldsymbol{\Upsilon}_{n,\alpha\beta}\, q_{n\beta} \tag{10}$$

which also replaces $\boldsymbol{\tau}_{n\alpha}$ in the definition of $\mathbf{f}_{nI,e}$. In expressions (5a) and (6), $\mathbf{f}_n(\mathbf{r}_n, t)$ is the force distribution acting on $\mathcal{B}_n$. Through these terms, the joint control forces, $\mathbf{f}_{n,c}$, and external forces, including interbody constraint forces, enter the equation of motion [30, 6]. We also point out that it is the $O(\|\mathbf{q}_{n,e}\|\ \|\boldsymbol{\nu}_n\|^2)$ term in $\hat{\mathbf{f}}_{nI,e}$, in particular the col $\{\boldsymbol{\omega}_n^T(\sum_{\beta=1}^{s_n} \boldsymbol{\Upsilon}_{n,\alpha\beta}\, q_{n\beta})\boldsymbol{\omega}_n\}$ term that is responsible for the well-known softening effect in the dynamics equations. It is a general discrete form of the softening term $\omega^2 q_r$ which is often cited for a planar beam rotating at angular speed ω.

The second group of the inertial nonlinear terms contains those terms which affect the mass matrices of the body as they represent "inertia of deformation." Thus, we define

$$\hat{\mathcal{M}}_{n,rr} = \mathcal{M}_{n,rr} + \delta\mathcal{M}_{n,rr} \tag{11}$$

$$\hat{\mathcal{M}}_{n,re} = \mathcal{M}_{n,re} + \delta\mathcal{M}_{n,re} \tag{12}$$

In the above, the constant rigid mass matrix is defined by

$$\mathcal{M}_{n,rr} \triangleq \begin{bmatrix} m_n 1 & -\mathbf{c}_n^{\times} \\ \mathbf{c}_n^{\times} & \mathbf{J}_n \end{bmatrix} \tag{13}$$

where m_n, $\mathbf{c}_n$, and $\mathbf{J}_n$ are the mass, first and second moments of inertia with respect to O_n, of the undeformed body. The constant part of the mass matrix, which couples rigid and elastic motions is

$$\mathcal{M}_{n,re} \triangleq \begin{bmatrix} \text{row}\{\mathbf{P}_{n\alpha}\} \\ \text{row}\{\mathbf{H}_{n\alpha}\} \end{bmatrix},\ \alpha = 1 \dots s_n \tag{14}$$

where $\mathbf{P}_{n\alpha} = \int_{\mathcal{B}_n} \boldsymbol{\psi}_{n\alpha} dm_n$ and $\mathbf{H}_{n\alpha} = \int_{\mathcal{B}_n} \mathbf{r}_n^{\times}\boldsymbol{\psi}_{n\alpha} dm_n$ are the elastic momentum and angular momentum coefficients.

The elastic dependence of the body mass matrix is accounted for by augmenting the first and second moments of inertia, as well as the angular momentum coefficient. This is done through $\delta\mathcal{M}_{n,rr}$ and $\delta\mathcal{M}_{n,re}$ which give rise to the hybrid terms of $O(\|\mathbf{q}_{n,e}\|\ \|\dot{\boldsymbol{\nu}}_n\|)$, $O(\|\mathbf{q}_{n,e}\|\ \|\ddot{\mathbf{q}}_{n,e}\|)$ and $O(\|\mathbf{q}_{n,e}\|^2\ \|\dot{\boldsymbol{\nu}}_n\|)$ in the motion equations. They are defined analogously to equations (13) and (14) with:

$$\delta \mathbf{c}_n = \sum_{\alpha=1}^{s_n} \mathbf{P}_{n\alpha} q_{n\alpha}$$

$$\delta \mathbf{J}_n = \sum_{\alpha=1}^{s_n} \left[-(\boldsymbol{\tau}_{n\alpha} + \boldsymbol{\tau}_{n\alpha}^T) q_{n\alpha} - \sum_{\beta=1}^{s_n} \boldsymbol{\Upsilon}_{n,\alpha\beta}\, q_{n\alpha}\, q_{n\beta} \right]$$

$$\delta \mathbf{H}_{n\alpha} = \sum_{\beta=1}^{s_n} \boldsymbol{\nu}_{n,\alpha\beta}\, q_{n\beta} \tag{15}$$

We observe that the argument of the second summation in (15*b*) is a quadratic function of elastic variables $q_{n\beta}$. Its inclusion is necessary to preserve the positive-definiteness of the augmented inertia matrix.

2.3 Geometric Nonlinearities

2.3.1 Nonlinear Elastic Force. Assuming small-strain, but not necessarily small-displacement deformation, the strain energy for a linearly elastic body takes the form:

$$U_{n,e} = \frac{1}{2} \int_{\mathcal{B}_n} \boldsymbol{\epsilon}^T \mathbf{D} \boldsymbol{\epsilon}\, dV_n \tag{16}$$

where $\boldsymbol{\epsilon}$ is a 6×1 column matrix with components of the Cauchy-Green strain tensor and $\mathbf{D}$ is a symmetric matrix depending on material properties. To derive the elastic forces or the stiffness term in the motion equations, we need to replace $\boldsymbol{\epsilon}$ in terms of displacements using the strain-displacement relations. The Green's strains specified in the underformed coordinates can be partitioned into the linear and the second-order nonlinear contributions:

$$\boldsymbol{\epsilon} = \boldsymbol{\epsilon}_L + \boldsymbol{\epsilon}_{NL} \tag{17}$$

Substituting the above into (16) gives the following expression for the strain energy:

$$U_{n,e} = \frac{1}{2} \int_{\mathcal{B}_n} (\boldsymbol{\epsilon}_L^T \mathbf{D} \boldsymbol{\epsilon}_L + 2\boldsymbol{\epsilon}_L^T \mathbf{D} \boldsymbol{\epsilon}_{NL} + \boldsymbol{\epsilon}_{NL}^T \mathbf{D} \boldsymbol{\epsilon}_{NL})\, dV_n \tag{18}$$

This form makes explicit the two additional terms in the strain energy that arise from the nonlinear component of the strain-displacement relation. They are a third-order term coupling the linear and nonlinear strains and a fourth-order term which involves the latter only. Several multibody dynamics formulations (for example, that in reference [21]) incorporate only the third-order contribution since it is this term that couples "axial" to "transverse" deformations, and therefore accounts for the foreshortening effect.

After substituting in (18) for strains in terms of the discretized displacements, we can obtain the elastic forces from the resulting strain energy by employing Castigliano's First theorem:

$$\hat{\mathbf{S}}_{n,ee} = \frac{\partial U_{n,e}}{\partial \mathbf{q}_{n,e}} \tag{19}$$

This elastic force vector can be factored into a symmetric stiffness matrix $\hat{\mathcal{K}}_{n,ee}$ and a column of elastic coordinates. If the assumed displacement field is linearized with respect to rotations, then we can express $\hat{\mathcal{K}}_{n,ee}$ as a sum of three terms, in accordance with the three contributions to the strain energy. These are: (i) a constant matrix, which is the conventional stiffness matrix employed in linear analysis; (ii) a first-order geometric stiffness and (iii) a second-order stiffness matrix and are defined so that:

$$\hat{\mathbf{S}}_{n,ee} \equiv \hat{\mathcal{K}}_{n,ee} \mathbf{q}_{n,e} = \left(\mathcal{K}_{n,0} + \frac{1}{2!} \mathcal{K}_{n,1} + \frac{1}{3!} \mathcal{K}_{n,2} \right) \mathbf{q}_{n,e} \tag{20}$$

with the subscripts distinguishing the order of the dependence on the elastic coordinates. This formulation of the elastic force leads naturally to a classification of the geometric *elastic* nonlinearities according to the order of the stiffness term. A similar breakdown of elastic nonlinearities was proposed in reference [25]. We also note that if one retains only the aforementioned third-order coupling term in the strain energy and substitutes for the axial displacement in it in terms of the axial load, which in addition is treated as constant, then the resulting geometric stiffness $\mathcal{K}_{n,1}$ takes a simpler, "pseudo-constant" form. In particular, it comprises terms that affect only the transverse degrees of freedom (and not the axial degrees of freedom) through the axial load. The latter is evaluated according to the initial substitution as a linear function of the time-dependent axial displacements.

2.3.2 Tip Deformation. The interbody geometric nonlinearities stem from the deformation of the "tip" of $\mathcal{B}_n$ with respect to the inboard articulation point. The deformed interjoint position vector is

$$\hat{\mathbf{r}}_{n,n+1} = \mathbf{r}_{n,n+1} + \sum_{\alpha=1}^{s_n} \boldsymbol{\psi}_{n\alpha}(\mathbf{r}_{n,n+1}) q_{n\alpha} \tag{21}$$

where $\mathbf{r}_{n,n+1}$ is the underformed position of the outboard articulation point O_{n+1} expressed in $\mathcal{B}_n$.

The rotation matrix from $\mathcal{B}_n$ to $\mathcal{B}_{n+1}$ can be written as

$$\mathbf{C}_{n+1,n} = \mathbf{C}_{n+1,n,r}(\theta_{n+1}) \mathbf{C}_{n,e}(\mathbf{q}_{n,e}) \tag{22}$$

The matrix $\mathbf{C}_{n+1,n,r}$ includes the effects of the joint angle θ_{n+1} at O_{n+1} (for a revolute joint) and $\mathbf{C}_{n,e}$ incorporates the elastic rotation of the tip of $\mathcal{B}_n$ with respect to the inboard articulation point. This latter matrix is the solution of

$$\dot{\mathbf{C}}_{n,e} = -\mathbf{C}_{n,e} \boldsymbol{\omega}_{n,e}^{\times} \tag{23}$$

where

$$\boldsymbol{\omega}_{n,e} = \sum_{\alpha=1}^{s_n} \boldsymbol{\theta}_{n\alpha}(\mathbf{r}_{n,n+1}) \dot{q}_{n\alpha}, \qquad \boldsymbol{\theta}_{n\alpha}(\mathbf{r}_{n,n+1}) \triangleq \frac{1}{2} \nabla^{\times} \boldsymbol{\psi}_{n,\alpha}(\mathbf{r}_{n,n+1}) \tag{24}$$

In the above, we have noted that $\boldsymbol{\omega}_{n,e} = \frac{1}{2} \nabla^{\times} \dot{\mathbf{u}}_{n,e}(\mathbf{r}_{n,n+1}, t)$ are the components of the angular velocity of the tip with respect to a local undeformed frame and expressed in this latter frame. This is an exact result, as noted in [31], independent of the size of the elastic displacements and rates. The price that is paid is that (23), or an equivalent parametrization, must be integrated in conjunction with the motion equations. Cardona and Geradin [28] and Simo and Vu-Quoc [27] parametrize the elastic rotation matrix, which is defined at each point in the body, in terms of the rotation axis/angle parameters, also referred to as a rotation vector. Furthermore, they discretize the corresponding rotation field,

as represented by the rotation vector, separately from the deformation field. In this case, integration of the rotational discrete coordinates yields tip attitude directly.

For small elastic displacements and rates, one can further write

$$\mathbf{C}_{n,e} = \mathbf{1} - \boldsymbol{\theta}^{\times}_{n,e},$$

$$\boldsymbol{\theta}_{n,e}(t) \triangleq \sum_{\alpha=1}^{s_n} \boldsymbol{\theta}_{n\alpha}(\mathbf{r}_{n,n+1})\, q_{n\alpha}(t) \quad (25)$$

which is directly obtainable from the elastic displacements $\mathbf{q}_{n,e}$. Implicit in this first-order approximation is the assumption that $\boldsymbol{\omega}_{n,e} = \dot{\boldsymbol{\theta}}_{n,e}$, i.e., a rotation can be treated as a vector. Other authors have assumed that $\boldsymbol{\theta}_{n,e}$, as defined in (25*b*), can be assigned to a particular sequence of Euler angles. For example, Kane et al. [9] assume a 1-2-3 Euler sequence. For noninfinitesmal displacements, however, $\mathbf{C}_{n,e}$ will depend on the order of rotation selected, a choice which may not be obvious for three-dimensional modelling and moreover, is arbitrary. In this case, identification of $\boldsymbol{\theta}_{n,e}$ as an Euler angle set precludes the equation of $\dot{\boldsymbol{\theta}}_{n,e}$ with $\boldsymbol{\omega}_{n,e}$. Hence, (24*a*) would be replaced with

$$\boldsymbol{\omega}_{n,e} = \mathbf{C}^{T}_{n,e}\, \mathbf{E}_n \dot{\boldsymbol{\theta}}_{n,e}$$

where $\mathbf{E}_n$ is the transformation from Euler rates to angular velocity (expressed in the *deformed* tip frame). It is further noted that for planar motion, (23) and the Euler angle interpretation are equivalent.

2.4 Kinematical Constraints for a Chain of Bodies. Thus far we have discussed the dynamics equations and local kinematics for an unconstrained elastic body. In order to describe the motion of the chain of interconnected bodies, we must impose the geometrical constraints between them. The kinematical relationship governing the generalized velocities can be written recursively [32] as

$$\boldsymbol{\nu}_{n+1} = \mathcal{T}_{n+1,n}\boldsymbol{\nu}_n + \mathcal{S}_{n+1,n}\dot{\mathbf{q}}_{n,e} + \mathcal{P}_{n+1}\dot{\boldsymbol{\theta}}_{n+1} \quad (26)$$

where

$$\mathcal{T}_{n+1,n} \triangleq \begin{bmatrix} \mathbf{C}_{n+1,n} & -\mathbf{C}_{n+1,n}\hat{\mathbf{r}}^{\times}_{n,n+1} \\ \mathbf{O} & \mathbf{C}_{n+1,n} \end{bmatrix},$$

$$\mathcal{S}_{n+1,n} \triangleq \begin{bmatrix} \mathbf{C}_{n+1,n}[\mathrm{row}\{\boldsymbol{\psi}_{n\alpha}(\mathbf{r}_{n,n+1})\}] \\ \mathbf{C}_{n+1,n}[\mathrm{row}\{\boldsymbol{\theta}_{n,\alpha}(\mathbf{r}_{n,n+1})\}] \end{bmatrix} \quad (27)$$

and $\mathcal{P}_{n+1}$ is a projection matrix which aids in expressing the generalized velocity induced by the joint motion. Although (26) has been written in a form restricted to single DOF revolute joints, this is simply for notational clarity. Multi-DOF joints encompassing translational and/or rotational behaviour are easily handled [6].

We observe that the kinematical constraints represented by (26) are an integral component of the solution procedure for the dynamics of the system when the motion equations are formulated using the floating frame approach. In the finite-element procedure of Simo and Vu-Quoc [33], where the dynamics equations are derived using the generalized coordinates measured with respect to the inertial frame, the kinematic constraints between bodies are implicitly ensured through the continuity or compatibility of the displacements at the interconnection joints.

It is through the generalized transformation matrices of (27) that the different approximations for tip deformation give rise to interbody nonlinearities. In keeping with the remarks of the previous section, four possible modelling approaches present themselves:

(*a*) Neglect the kinematical nonlinearities which accrue from elastic deformation. This is equivalent to setting $\mathbf{C}_{n+1,n} \equiv \mathbf{C}_{n+1,n,r}(\boldsymbol{\theta}_{n+1})$ and $\hat{\mathbf{r}}^{\times}_{n,n+1} = \mathbf{r}^{\times}_{n,n+1}$ in Eq. (27).

(*b*) Model the elastic effects to first order by using the approximation (25) and the exact expression (21) for the interjoint position.

(*c*) Take the elastic rotations $\boldsymbol{\theta}_{n,e}$ to represent an Euler angle sequence. In this case, the bottom partition of $\mathcal{S}_{n+1,n}$ must be modified to read

$$\mathbf{C}_{n+1,n,r}\mathbf{E}_n[\mathrm{row}\{\boldsymbol{\theta}_{n,\alpha}(\mathbf{r}_{n,n+1})\}]$$

and $\mathbf{C}_{n,e}(\boldsymbol{\theta}_{n,e})$ must be constructed appropriately.

(*d*) Use the exact modelling implied by (21) and (24) and integrate (23) for the true orientation of the tip, $\mathbf{C}_{n,e}$.

The recursive relationship governing the generalized acceleration can be acquired by differentiating (26):

$$\dot{\boldsymbol{\nu}}_{n+1} = \mathcal{T}_{n+1,n}\dot{\boldsymbol{\nu}}_n + \mathcal{S}_{n+1,n}\ddot{\mathbf{q}}_{n,e} + \mathcal{P}_{n+1}\ddot{\boldsymbol{\theta}}_{n+1} + \dot{\mathcal{T}}_{n+1,n}\boldsymbol{\nu}_n + \dot{\mathcal{S}}_{n+1,n}\dot{\mathbf{q}}_{n,e} \quad (28)$$

The particular form of the matrices $\dot{\mathcal{T}}_{n+1,n}$ and $\dot{\mathcal{S}}_{n+1,n}$ depends on the kinematical modelling adopted.

2.5 Solution Procedure. A solution of the simulation dynamics problem requires determination of $\{\ddot{\boldsymbol{\theta}}_n, \ddot{\mathbf{q}}_{n,e}\}$ at each time step given the control torques at each joint. In general, this can be accomplished via two families of procedures—global techniques and recursive ones. The results given in this paper have been computed using the recursive dynamics procedures documented in [32] and [34]. The major difference between the two methods revolves around the elimination of the generalized interbody forces from the motion equations. According to the algorithm of D'Eleuterio [32, 8], one eliminates the constraint component of the interbody force by assuming it to be an affine function of the generalized accelerations. In the other procedure, the net (constraint plus control) interbody force is removed in a similar manner. Two independent computer codes implementing the two recursive algorithms have been written and validated against each other. The nonlinear terms, as presented, do not alter the basic form of the key relationships (3) and (28) which form the basis of most recursive algorithms.

Once the independent accelerations $\{\ddot{\boldsymbol{\theta}}_n, \ddot{\mathbf{q}}_{n,e}\}$ for $n = 1, \ldots, N$ are known, they can be directly integrated for the velocities and displacements of the system. This can be accomplished with a variety of numerical integration methods for initial-value problems. In our simulation, we have employed the routine LSODE. The numerical results presented in Section 4 were generated using the nonstiff option of LSODE, which implements Adams multistep formulas. It was found that the stiff option of LSODE provides identical results but at a considerably higher computational cost.

3 Simulation Models

3.1 Approximate Dynamics Models. In Section 2, we put forward a classification of the nonlinear terms that arise in the dynamics equations of a multibody system into three categories: inertial, geometric elastic, and geometric interbody. The first two were further subdivided into two and three groups, respectively, and we proposed four methods for modeling the interbody kinematics. The latter introduce nonlinearities into the dynamics model of the whole system, rather than each body. Clearly, depending on the nonlinear terms retained in the body dynamics equations and the approximation used for the interbody constraints, one can derive a number of approximate models. Among these, we will present numerical results for the selected four.

Our first and simplest model is one defined by a ruthless linearization of the dynamics equations. It contains none of the inertial, nor elastic, nor interbody nonlinearities and is therefore defined using the constant body matrices and the "unhatted" forcing terms in the motion equations (3). Accordingly, in the kinematics constraints employed with these equations we neglect the elastic deformation at the tip. Following Padilla and von Flotow [20], we refer to this model as ruthlessly linearized and denote it by RL.

The second model worthy of separate designation is the one which we call inconsistent (I). It incorporates all of the inertial nonlinearities, but neglects the geometric elastic nonlinearities. This model is very similar to the inconsistently linearized (IL) model of Padilla and von Flotow, which in turn forms the basis of the majority of multibody dynamics codes. The main difference between the two is that the inconsistent model includes second-order mass matrix corrections (and therefore is not linear), while these terms are lacking from the corresponding linearized model. This inconsistent approximation of the dynamics equations is usually combined with the first-order interbody kinematics as described in (b) of Section 2.4. However, in our numerical examples we also present results for this model in combination with the other two descriptions of the interbody kinematics—the 3-2-1 and 1-2-3 Euler sequences according to specifications in (c) of Section 2.4, and the exact model for the tip deformation as described in (d). These will be denoted by I(1-2-3), I(3-2-1), and I(E).

The third model considered here is the consistently linearized approximation. It includes the inertial hybrid forcing terms (without mass matrix corrections) and the geometric stiffness matrix derived under the constant axial load assumption. The corresponding dynamics equations are similar to the consistent linear equations of Simo and Vu-Quoc [10], as well as Kane et al. [9] and Ider and Amirouche [21]. The tip deformation for the interbody kinematics is modelled to first-order and the resulting model is denoted by CL.

Finally, as expected, our last model is based on the "exact" dynamics equations for an elastic body which include all of the inertial and geometric elastic nonlinearities. The nominal description of the interbody kinematics employed with these equations will be, naturally, the exact geometrical model of (d) in §2.4, although we will also investigate their performance in conjunction with the linear and Euler sequence approximations. The resulting models will be referred to as EEE, EE(1), EE(3-2-1) and EE(1-2-3). The allocation of geometric nonlinearities among the models I, CL, and EE, is similar to that used by Mayo and Dominguez [25] in forming their three models. Their study used existing multibody dynamics software and hence the inertial and kinematical nonlinearities were the same for each model. The models were termed "linear," "partially nonlinear," and "completely nonlinear."

3.2 Spatial Discretization for Slender Bodies. An important aspect of the modelling process concerns the procedure employed to discretize the elastic links of the manipulator. There exist several techniques, the most common of which are the finite element method and the modal expansion method [35, 36]. Both procedures were employed to generate the models used in the next section. Through implementation of both methods, we have gained an additional understanding of the more subtle characteristics of these techniques, which are not apparent otherwise.

Our choice of the finite element method was motivated by the fact that this procedure is often touted for its generality and ease of implementation. In particular, flexible links with nonuniform mass and stiffness distributions are readily treated. The finite element scheme allows one to discretize bodies with complex shapes—an attribute which stems from the availability of structural elements that can approximate different geometries. Moreover, one can use the finite element procedure to discretize the rotation field independently from the displacement field—an advantage critical for finite-rotation models. By contrast, the eigenfunctions are primarily used for those models which permit an analytical solution for the natural modes.

In the context of space manipulator dynamics, the generality of the finite element scheme is usually a redundant feature, since the flexible links of manipulators are well-(and most often) approximated by Euler-Bernoulli beams. Since the differential equations lead to analytical solutions for the eigenmodes, they can be used to discretize the elastic links, with some advantages. For example, by using a specific number of eigenfunctions, one is assured of reproducing exactly the corresponding constrained natural frequencies. In the finite element scheme, however, one needs to use more than one element in order to obtain an acceptable approximation for a particular frequency. This in turn leads to the introduction of extra nodal coordinates, along with high and spurious frequencies. These have several detrimental effects on the dynamics simulation, such as degradation of the efficacy of integration, increased dimensionality of the state and numerical noise. With regard to ease of implementation, we have found that using the eigenfunctions to model the elastic links is no more difficult than employing the finite element procedure. In this light, we suggest that the eigenfunction expansion is at least as attractive as the finite element scheme for discretizing the links of manipulators in the case where simple beam theories provide a suitable approximation for the elastic behaviour of the links.

In view of the application considered here, the two discretization techniques are presented for a slender body, in particular the Euler-Bernoulli beam. Thus, both schemes are applied to the linearized displacement field of the form:

$$\mathbf{u}_{n,e} = \begin{bmatrix} u_0 - y\dfrac{\partial v_0}{\partial x} - z\dfrac{\partial w_0}{\partial x} \\ v_0 - z\phi_0 \\ w_0 + y\phi_0 \end{bmatrix} \tag{29}$$

where the quantities u_0, v_0, and w_0 refer to the displacements of the centroidal axis and ϕ_0 is the twist angle. The above expression assumes that the rotation distribution due to elasticity is given by $\{\phi_0, dv_0/dx, dw_0/dx\}$ which are interpreted as small angles. Therefore, we do not discretize the rotations independently of the displacements and as a consequence, neglect shear deformation a priori. The complete dynamics equations that result from the linearized displacements (29) are of third-order in the elastic coordinates. In the approach of Simo and Vu-Quoc, the analogous approximation in the dynamics model can be introduced by approximating the nonlinear strain measures. Indeed, it can be shown that the strain energy derived as described in Section 2.3.1 for the displacement field (29) is identical to the strain energy emanating from the second-order approximation for strain measures in reference [10], with the additional assumption of negligible shear deformation. In spite of its approximate character, the present approach should be quite accurate for links of sufficient slenderness.

Let us now outline the two discretization techniques used to model flexible links of a manipulator. In the finite element method the element we have employed to model the deformation of the links is the beam element [37]. The elastic displacement at any point in the element is related to the deformations at the two nodes through the matrix of basis functions: $\mathbf{u}_e = \mathbf{\Psi}_e \mathbf{q}_e$, where $\mathbf{\Psi}_e$ has the standard form [37, p. 293] which is consistent with (29) and $\mathbf{q}_e$ is the 12 × 1 column of elemental nodal displacements. Here, the subscript $(\cdot)_e$ connotes "elemental" and we have dropped the body index n to simplify the notation.

The modal expansion—our second discretization scheme—is defined by:

$$\mathbf{u}_e(\mathbf{r}, t) = \sum_{\alpha=1}^{s_u} \begin{bmatrix} u_\alpha \\ 0 \\ 0 \end{bmatrix} q_{u\alpha}(t) + \sum_{\alpha=1}^{s_v} \begin{bmatrix} -y\dfrac{\partial v_\alpha}{\partial x} \\ v_\alpha \\ 0 \end{bmatrix} q_{v\alpha}(t)$$

$$+ \sum_{\alpha=1}^{s_w} \begin{bmatrix} -z\dfrac{\partial w_\alpha}{\partial x} \\ 0 \\ w_\alpha \end{bmatrix} q_{w\alpha}(t) + \sum_{\alpha=1}^{s_t} \begin{bmatrix} 0 \\ -z\phi_\alpha \\ y\phi_\alpha \end{bmatrix} q_{t\alpha}(t)$$

where $v_\alpha(x) = w_\alpha(x)$ are the normalized bending mode shapes of a cantilevered uniform Euler-Bernoulli beam, and the functions $u_\alpha(x)$ and $\phi_\alpha(x)$ are the normalized stretching and torsional mode shapes of a uniform rod.

Once the basis functions have been specified, the mass and stiffness matrices for the links and the various integrals of the basis functions required for evaluation of the motion equations can be derived. In the finite element procedure, the assembly of the constant body matrices $\mathfrak{M}_{n,ee}$, $\mathcal{K}_{n,0}$ for each flexible link is carried out in the standard manner from the elemental matrices. During the assembly we also delete the columns and rows which correspond to the constrained nodal degrees of freedom. For the eigenfunction expansion scheme, the elastic mass and stiffness matrices have the simple diagonal forms $\mathfrak{M}_{n,ee} = \text{diag}\{1\}$, $\mathcal{K}_{n,0} = \text{diag}\{\omega_{n\alpha}^2\}$ where $\omega_{n\alpha}$ are the natural frequencies of the body in isolation and cantilevered at the inboard articulation point. The geometric stiffness matrices for either discretization scheme are assembled during the simulation procedure according to the appropriate expressions in terms of elastic coordinates. These can be obtained according to the procedure outlined in Section 2.3.1 with the strain energy expression of the form given by Hanagud and Sarkar [38], adapted to allow for nonplanar bending and small twisting deformation.

4 Numerical Results

4.1 Single Flexible Beam. The first numerical example treats a planar spin-up maneuver for a pinned free beam which permits examination of all four model classes independent of interbody constraints. The structural model is adapted from reference [38] which in turn is based on [9]. A planar spin-up beam example is also presented in references [11] and [21]. We consider a homogeneous isotropic beam of constant cross-section with properties

$$m = 12\ \text{kg}, \quad l = 10\ \text{m}, \quad A = 4.601 \times 10^{-4}\ \text{m}^2$$

and elastic stiffnesses

$$EI = 1.4004 \times 10^4\ \text{N} \cdot \text{m}^2, \quad EA = 3.1724 \times 10^7\ \text{N}$$

The beam is modeled with a single planar beam element in the finite-element discretization, and with two bending and one stretch modes in the eigenfunction expansion scheme. The maneuver presented here is "torque-driven" rather than "displacement-driven." The applied torque at the pinned end is calculated using the inverse dynamics procedure for a rigid model of the link, with the prescribed trajectory:

$$\dot{\theta}_1(t) = \begin{cases} 6\left(\dfrac{t}{T} - \dfrac{1}{2\pi}\sin\dfrac{2\pi t}{T}\right)\text{rad/s}, & 0 \le t \ge 15\text{s} \\ 6\ \text{rad/s}, & t \ge 15\ \text{s} \end{cases}$$

The above trajectory is identical to that used in the displacement-driven beam example in references [9, 11, 21, 38].

In general, the validity of the selected models can be assessed by measuring the error in the energy balance for the system. We use the root mean square value of the percentage energy balance error, $e_{E,\text{RMS}}$, the latter calculated at time t_i as:

$$e_E(t_i) = \frac{E(t_i) - W(t_i)}{|E_{\text{peak}}|} \times 100\% \tag{30}$$

In the above, E is the total energy of the system, E_{peak} denotes the maximum (peak) total energy reached during the maneuver and W is the work done on the system by the control forces. This work is equal to the integral of the power input over the elapsed time, that is:

$$W = \int_0^{t_i} \pi\, dt, \quad \pi = \sum_{n=1}^{N} f_{n,c}\dot{\theta}_n \tag{31}$$

The RMS value of the percentage energy drift is then determined according to:

Table 1 RMS energy drift for single flexible beam example

Discretization	Model RL	Model I	Model CL	Model EE
FE	2.47×10^{-3}	5.35×10^{-5}	0.159	1.40×10^{-5}
NM	3.32×10^{-3}	5.90×10^{-5}	0.220	8.47×10^{-6}

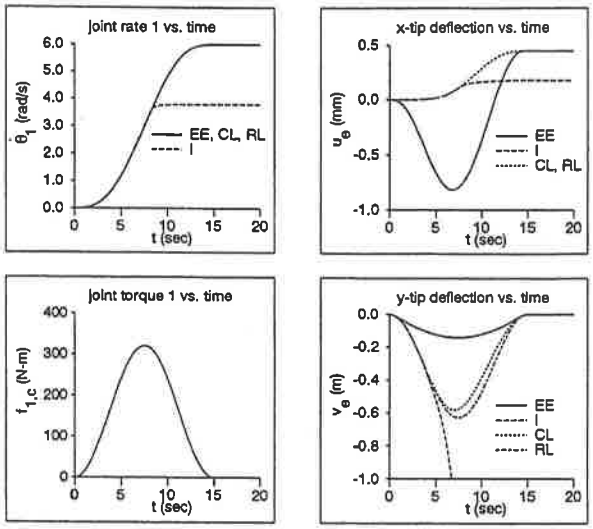

Fig. 1 Simulation results for single flexible beam

$$e_{E,\mathrm{RMS}} = \sqrt{\frac{\sum_{i=1}^{1000} e_E(t_i)^2}{1000}} \tag{32}$$

The values of $e_{E,\mathrm{RMS}}$ obtained with the four dynamics models and two discretization schemes are summarized in Table 1. As can be seen, the results observed using the natural modes (NM) and a beam element (FE) show the same trends and are of the same order of magnitude.

According to the above, the inconsistent model does almost as well as the exact model, despite the fact that the solution it provides is clearly implausible (see Fig. 1). The reason why the I model predicts such a "good" energy drift is because it contains the elastic configuration dependence in the mass matrix given in (15). Indeed, without these terms, the value of $e_{E,\mathrm{RMS}}$ increases to 23.8 with no discernible difference in the simulation results. The CL model does poorly according to the energy drift measure because strain energy is lost as a result of using a "constant axial load" assumption in the geometric stiffness for this model. We also note that including the mass matrix correction terms in the CL model does not significantly improve the energy drift.

As can be seen from the joint rate plot in Fig. 1, the EE, CL, and RL models yield solutions that are very similar to the prescribed trajectory, while the inconsistent model levels off prematurely. The steady-state stretch displacement (u_e) is almost identical for the former three models, whereas the inconsistent model appears to underestimate it. The exact modeling predicts an intermediate compression of the beam stemming from the nonlinear coupling to the bending displacement; this is the foreshortening effect. When the CL model is used, the beam does not foreshorten because, as alluded to earlier, the linear geometric stiffness employed in this model does not account for the effect of bending on the axial displacement.

Table 2 Properties of the SRMS

Property	l (m)	Mass (kg)	J_n^r (kg·m^2)	J_n^p (kg·m^2)	J_n^y (kg·m^2)
Space shuttle	—	93,270	1.17×10^6	9.1×10^6	9.5×10^6
Link 1	0.9	95.0	0.2	25.75	25.75
Link 2	6.4	138.0	0.4	1884.36	1884.36
Link 3	7.0	85.0	0.4	1388.53	1388.53
Link 4	0.5	8	0.2	0.76	0.76
Link 5	0.8	44	0.2	9.49	9.49
Link 6	0.6	41	0.2	5.02	5.02
Payload	—	15,000	30,000	515,000	515,000

Elastic stiffnesses	EI (N • m^2)	GJ (N • m^2)	EA (N)
Link 2	4.046×10^6	2.040×10^6	2.790×10^9
Link 3	2.812×10^6	1.417×10^6	1.194×10^9

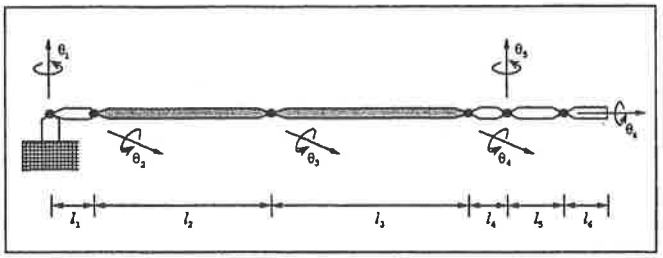

Fig. 2 Architecture of the SRMS

The ruthless and consistent models provide similar curves for the bending displacement which are in close agreement with the previously published results (see, for example Ider and Amirouche [21]). The lack of visible oscillatory motion in our results is due to the fact that the maneuver is torque-driven. The exact results, which confirm those presented by Hanagud and Sarkar [38], show a reduced bending deformation because of the additional stiffening provided by the second-order stiffness matrix. The inconsistent model is totally inadequate since an extension of the plot reveals a steady-state bending displacement of 9 m. Thus, our results for a single flexible beam support the conclusions made by Padilla and von Flotow [20] regarding the validity of the ruthless, inconsistent and consistent models. However, we postpone making any generalizations based on this very special and simple system, until a multi-DOF, three-dimensional flexible manipulator is examined. In fact, we are of the opinion that the above example has formed a faulty basis for interpreting the importance of the geometric stiffening effect as well as advocating the capability of the ruthless model.

4.2 Shuttle Remote Manipulator System. The goal of the present section is to evaluate the performance of the models introduced in Section 3.1 on a six-degree-of-freedom manipulator, modelled after the Space Shuttle Remote Manipulator Arm. Included in the model is the space shuttle—body $\mathcal{B}_0$ of the chain—although, for the numerical results presented here, its motion is constrained. Furthermore, the arm is assumed to carry a payload, modelled by a cylindrical drum to represent a spin-stabilized satellite.

The properties of the members of the system are summarized in Table 2 and the architecture of the arm is shown in Fig. 2. We point out that the space shuttle and the payload

Table 3 RMS energy drift for SRMS example

Maneuver	Model RL	Model CL	Model I(E)	Model EEE
I-f	∞	∞	4.32×10^{-5}	2.57×10^{-4}
I-s	12.2	1.57×10^{-4}	2.10×10^{-7}	6.41×10^{-7}
II-f	∞	∞	2.71	5.82
II-s	∞	∞	33.7	22.3

are approximated by rigid bodies. The only flexible bodies are links 2 and 3 which are the lower and upper arm booms. Their fundamental frequencies are 37.2 rad/s and 34.5 rad/s, respectively.

The comparison of the different models will be done for two classes of maneuvers as described below.

I. The maneuvers in this category are generated with the control torques calculated using the inverse dynamics equations for the rigid-body model of the arm, with the prescribed joint angles parametrized by:

$$\theta_n(t) = \theta_d\left(\frac{t}{T} - \frac{1}{2\pi}\sin\frac{2\pi t}{T}\right), \quad n = 1, \ldots, 6 \qquad (33)$$

The trajectory of the form (33) for the duration time T represents a generic "pick-and-place" maneuver, whereby the manipulator starts from rest, accelerates gradually and then decelerates to a stop. The speed of maneuver for a fixed θ_d is determined by the value of T.

II. This class of maneuvers is defined by directly specifying the joint control torques. Unlike the smooth inputs for maneuvers I, the joint torques here are step functions, defined by:

$$\mathbf{f}_c(t) = \begin{cases} [f_{1,c}, \ldots, f_{6,c}]^T, & 0 < t < T/2 \\ \mathbf{0}, & T/2 \le t \end{cases} \qquad (34)$$

Clearly, the manipulator's trajectory and the maneuver's speed are determined by the magnitudes of $f_{n,c}$.

For each of the above categories we consider two maneuvers—slow (s) and fast (f)—each obtained by scaling the appropriate parameters in Eq. (33) and (34). These are chosen as follows:

I. $\theta_d = 0.4$ rad for maneuvers I-f and I-s;

II. $\mathbf{f}_{c,f} = [2, 3.5, 2, 1, 0.5, 0.01]^T$ kN-m and $\mathbf{f}_{c,s} = 1/10\,\mathbf{f}_{c,f}$ for maneuvers II-f and II-s, respectively.

The durations of the two maneuvers in each category are: $T_f = 20$ s and $T_s = 60$ s. We note that the maximum joint rate reached during the fastest of the above maneuvers is 0.04 rad/s which is three orders of magnitude lower than the fundamental frequencies of the booms. The maximum end-effector speed occurs for maneuver I-f and is 1.3 m/s. It is approximately an order of magnitude higher than the present speed attained during operation of the shuttle arm.

The values of $e_{E,\mathrm{RMS}}$ obtained with the four dynamics models of Section 3.1 for the four maneuvers are summarized in Table 3. The numbers cited here correspond to modelling of the two flexible booms using the natural modes for discretization with the relative local error tolerance for the numerical integration set to 10^{-7}. Each boom is modelled with six modes: two bending modes in each of the in-plane and out-of-plane directions, one stretch mode, and one torsional mode. Finite element modelling of the beams, using one element for each link, shows the same trends as the values in Table 3.

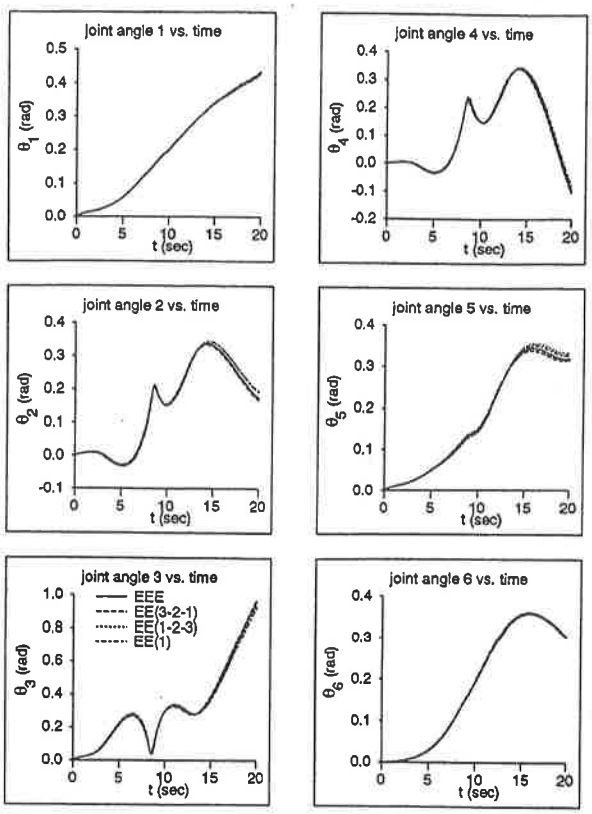

Fig. 3 I-f Simulation results for SRMS (model EE)

The simulations using models RL and CL for Maneuvers I-f, II-f, and II-s failed to finish owing to floating point overflow conditions. For instance, maneuver I-f "blows up" at 18.5 seconds for the ruthlessly linearized model and at 6.1 seconds for the consistently linearized model. Hence, the value of $e_{E,\mathrm{RMS}}$ has been tabulated as ∞ in Table 3. From the table we conclude that there is little to distinguish the inconsistent and exact models for all maneuvers on the basis of energy drift. For maneuver I-s—the only case where RL and CL models produce results for the complete trajectory—the high energy drift for the former indicates the doubtfulness of the solution. Although the drift for the CL simulation of this maneuver is not as good as that for the EEE (or I(E)) model, an inspection of the corresponding joint angles will reveal little difference between them.

The joint angle histories for maneuver I-f are given in Fig. 3 for the EE model. The four kinematical schemes of Section 2.4 yield similar behavior but there are discernible differences in the last 5 seconds of the simulation. More surprising are the results for the I model given in Fig. 4. The influence of the elastic kinematics breaks down into two distinct groupings. The exact and 3-2-1 Euler sequence yield similar curves while the linear approximation and 1-2-3 sequence provide completely different behavior. These curves would suggest that a 3-2-1 approximation—the torsional rotation is performed "last"—is superior to 1-2-3 sequence if integration for the elastic tip attitude is to be avoided. They also indicate that it is the omission of the stiffening terms in the inconsistent model which amplifies the differences in how the tip rotation is handled. Indeed, this

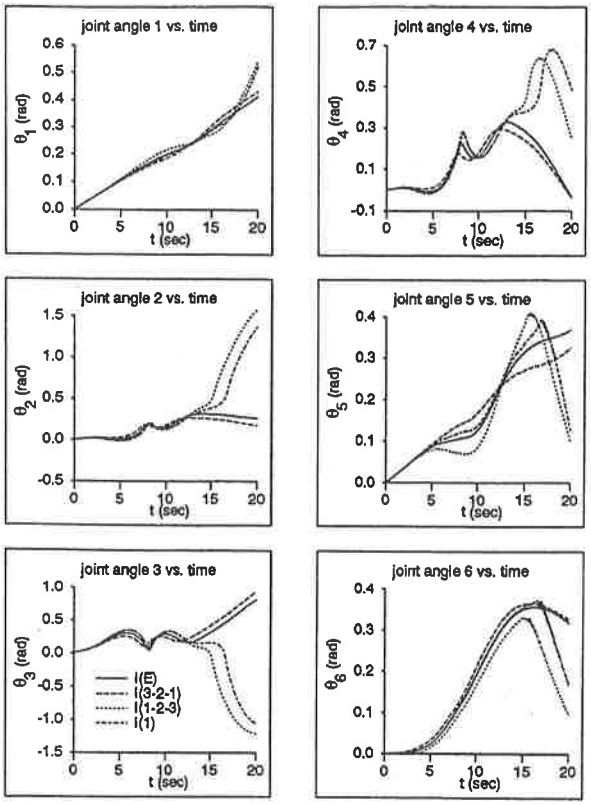

Fig. 4 I-f Simulation results for SRMS (model I)

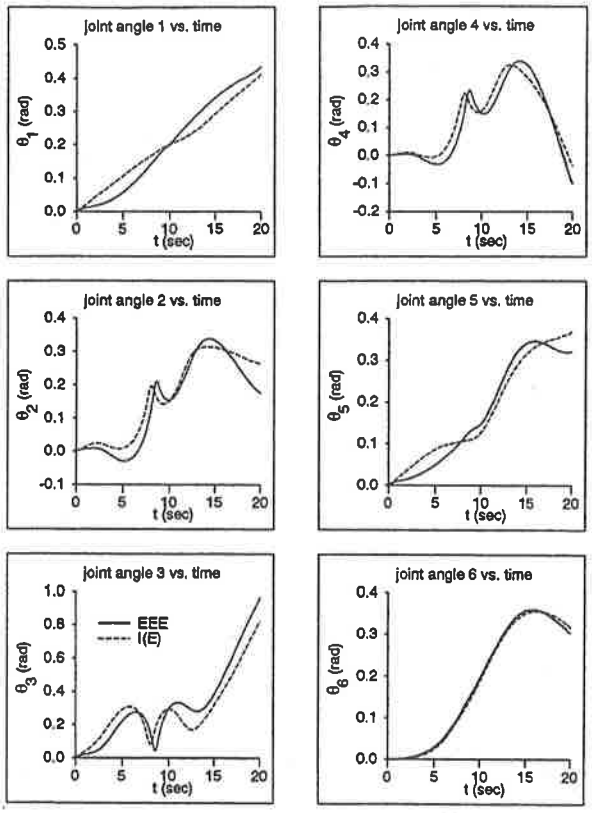

Fig. 5 I-f Simulation results for SRMS (models I(E) and EEE)

is in accordance with our expectations, since the geometric stiffening terms effectively increase the bending stiffness of the links (hence the term "stiffening") and consequently, the stiffened (EE) model predicts smaller elastic deformations than the inconsistent one. In Fig. 5, we have regraphed the EEE and I(E) results to emphasize the role of geometric stiffening on the joint angles. These evidently make a substantial difference, even though the joint rates are much lower than 10% of the fundamental frequencies of the elastic booms. Moreover, one could not have predicted such a discrepancy from the corresponding energy drift values. Additional insight into the geometric modelling can be gleaned from Fig. 6 where the tip deflections of links 2 and 3 are given for the I(E) and EEE models. The foreshortening of both links is clearly captured in the EEE case, but not by the I(E) model which also exaggerates the transverse bending.

A comparison of the modal expansion discretization with the finite element method for maneuver I-f is given in Fig. 7. For the latter method, two beam elements per link were used while for the modal technique, we employed three bending modes per transverse axis and two stretching modes. For both schemes, the torsional degrees of freedom were suppressed and the results were generated using the EEE model. The solutions are in good agreement between the two methods. Similar agreement was noted when torsion was included in the modelling of the booms. Discrepancies between these discretization schemes have been noted in [25] for the "completely nonlinear" model. They attributed them to the differences in the axial shape functions—piecewise linear ones versus smooth ones—since for the nonlinear elastic models, small changes in the axial behaviour can have a major impact on the transverse displacement.

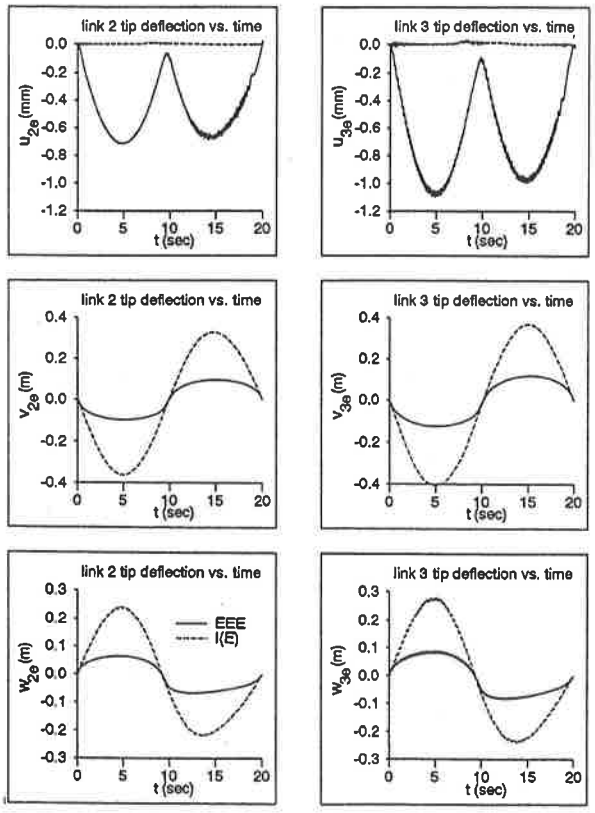

Fig. 6 I-f Boom deflection results for SRMS (models I(E) and EEE)

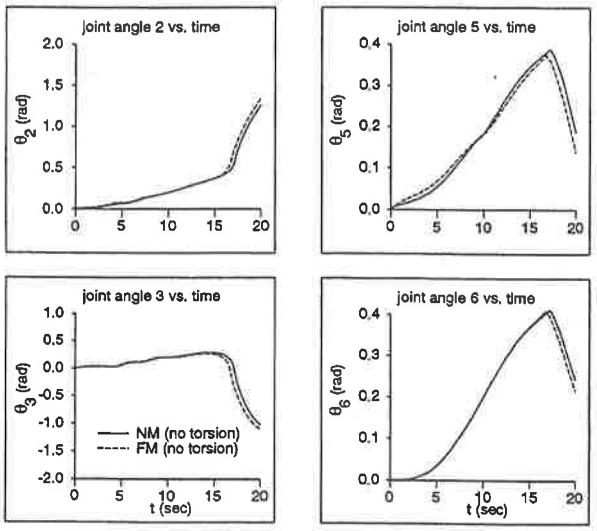

Fig. 7 I-f Simulation results without torsion (model EEE)

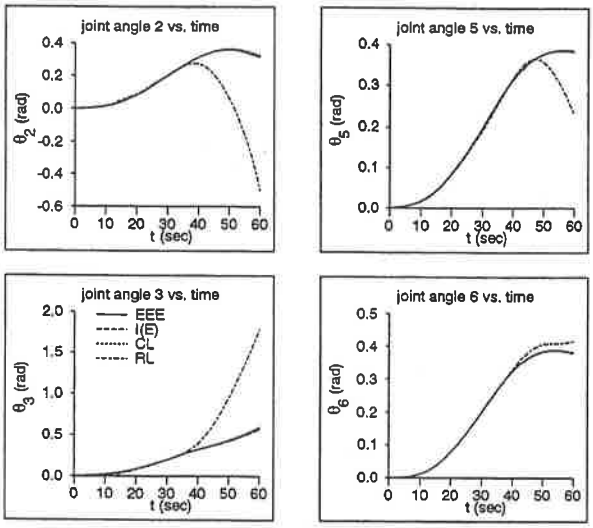

Fig. 8 I-s Simulation results for SRMS

Interestingly, the series of plots in Fig. 7 has a strong resemblance to the I(1) (and I(1-2-3)) curves of Fig. 4 where, we recall, the torsion is modelled and the dynamics equations lack the stiffening terms. One possible interpretation is that the 1-2-3 and linear kinematical schemes fail to properly capture the torsional deformation.

Four of the joint angles for maneuver I-s are given in Fig. 8. Models I, EE, and CL give almost identical results, independent of the method used to describe the rotational kinematics of the tip of links 2 and 3. This is consistent with the results of [25] for a slider-crank mechanism. For low crank rotational rates, the three models used exhibited similar slider deformations but as the crank rate was increased, divergences were noted. An analogous phenomenon was observed here since the CL model failed for the I-f run. For the current maneuver, the RL model generates radically different results and examination of the joint rates revealed an instability, which is also reflected in the relatively large value of $e_{E,\mathrm{RMS}}$ in Table 3. This particular run demonstrates vividly the importance of verifying the simulation results

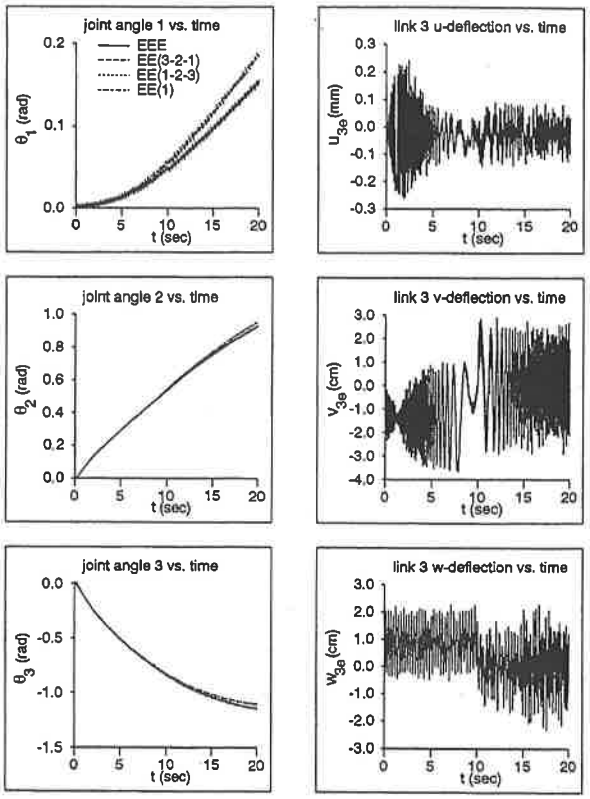

Fig. 9 II-f Simulation results for SRMS

with a physically meaningful measure, such as the energy drift for the system. However, as evidenced by maneuver I-f and the single beam results for models I(E) and EEE, the energy check by itself is not sufficient to validate the solution.

Three of the joint angle profiles for maneuver II-f are shown in Fig. 9 where only the results for EE have been presented. The EEE profiles are graphically identical to the EE(3-2-1) and EE(1-2-3) models as well as the corresponding inconsistent models which are not shown. The linear tip kinematics, however, produces substantially different joint angles in both the exact and inconsistent dynamics equations. This shows again that linearization with respect to the elastic rotations may fail to provide a good approximation. As previously noted, the ruthless model (RL) and the consistent model (CL) fail to finish this maneuver when the natural modes discretization scheme is used. However, the finite element method does produce results in the CL case, albeit very poor ones, with energy violation of 32%.

Finally, we observe that the energy drift values for the II-s maneuver are very high and lead one to suspect the results. By reducing the relative local error tolerance in the integrator routine from 10^{-7} to 10^{-12}, the value of $e_{E,\mathrm{RMS}}$ was reduced from 22.3 to 3.5×10^{-7}. Reduction of the tolerance for the previous runs reduced the values of $e_{E,\mathrm{RMS}}$ given in Table 3, but did not cause any of the runs which terminated prematurely to behave differently. Furthermore, the appearance of the graphs hitherto presented was unchanged. The first three joint angles and the tip deflections of link 3, which are given in Fig. 10 for the II-s maneuver, were obtained using the lower error tolerance. The results presented correspond to the EE models but the I models yield

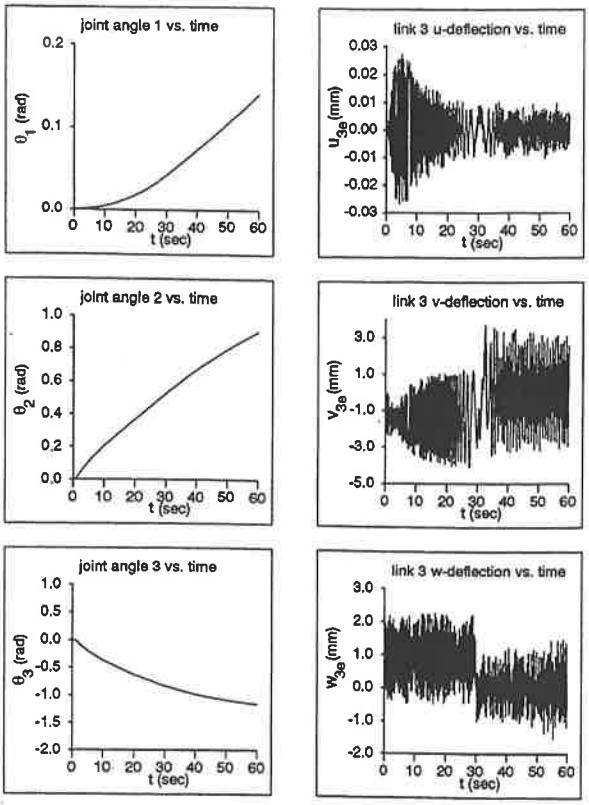

Fig. 10 II-s Simulation results for SRMS

no discernible difference, independent of the kinematical approach adopted. The lower tolerance was also used for the results given in Fig. 9 where the elastic deflections of link 3 for the II-f maneuver are also given. Contrary to the I-f and I-s runs, the step-driven deflection exhibit significant structural vibrations.

5 Concluding Remarks

In this work, several aspects of the dynamics modelling and simulation of flexible manipulators have been discussed. We presented and classified the inertial and geometric nonlinearities that arise in the motion and constraint equations for multibody systems. Subsequently, four models were proposed ranging from the simplest approximation in which none of the nonlinear terms are retained to the exact model where all terms originating from the fundamental nonlinear kinematics relations are included. It is clear from the results that both the inertial and geometric nonlinearities can have a profound effect on the simulation. It is hoped that the paper serves to partially answer the question "which terms in the motion equations are important?"

Although the specifics of the results will change when different manipulator systems are considered, we can make a few generalizations based upon our findings for a general 6-DOF manipulator. For sufficiently fast maneuvers of a realistic duration, the ruthlessly linearized approximation to the manipulator dynamics is wholly inadequate. In many cases, the deficiencies can be compensated for by including the nonlinear inertial forces which gives the inconsistently linearized model. The consistent model, which incorporates most of the inertial nonlinearities and the "first-order" stiffening term, performs as poorly as the ruthless model. These results are radically different from what one observes for a single beam or a planar two-link manipulator and hence, they are contrary to the findings of Padilla and von Flotow [20]. We suggest that the ruthless model, strongly advocated in the aforementioned reference, fails to provide a satisfactory approximation for the dynamics simulation of a general manipulator system. On the other hand, the inconsistent model presents an alternative set of equations which yields reliable simulations for a wide range of maneuvers and joint speeds. In many cases, it yielded reasonable results when both the ruthless and consistent models failed. We also discovered that the additional inclusion in the I model of the elastic coordinate dependence in the mass matrix insures its positive-definiteness and significantly reduces the magnitude of the energy drift.

It was shown in the paper that the geometric stiffening terms may have a considerable effect on the solution even in cases where the fundamental frequencies of the elastic links are well below the 10% value of the angular speeds. We have also demonstrated the necessity of retaining the third-order stiffening terms in the dynamics equations and not only the geometric stiffness that couples axial to transverse deformation, as done in several multibody formulations.

In terms of modeling tip deformation for the interbody kinematics, our numerical results proved that the common assumption of infinitesimal elastic rotations is not appropriate for simulating faster maneuvers. In fact, a linear approximation was often unreliable when compared with an exact solution. However, treating the rotations as the elements of an Euler sequence yielded reasonable results. In particular, we suggest that a 3-2-1 sequence for beams may be superior to a 1-2-3 choice when torsional degrees of freedom are present. The consequences of this are important since a "good" Euler sequence will allow one to avoid the exact treatment which requires numerical integration for the "tip" attitude. We also observed that inclusion of stiffening in the dynamics model mitigates the differences between various kinematical schemes.

With regard to the spatial discretization of the equations of motion, potential advantages associated with the eigenfunction expansion method for uniform beam models were noted. Both the finite element and modal expansion schemes were applied to model flexible links of a manipulator and the two methods were found to be in good agreement. Perhaps, the best solution for modeling of general flexible manipulator systems is the finite element method combined with model order reduction on a body by body basis.

References

1 Gaultier, P.E. and Cleghorn, W.L. "Modeling of Flexible Manipulator Dynamics," 1st National Applied Mechanisms and Robotics Conference, Cincinnati, OH, I, AMR-2C-3, Nov. 1989.

2 Bae, D.S., and Haug, E.J. "A Recursive Formulation for Constrained Mechanical System, Part I—Open Loop," *Mechanics of Structures and Machines*, Vol. 15, 3, 1987, pp. 359–382.

3 Serna, M.A., and Bayo, E. "A Modified Lagrangian Formulation for Elastic Robots," *Proc. 2nd International Symposium on Robotics and Manufacturing: Research, Education, and Applications*, New Mexico, 1987, pp. 513–520.

4 Naganathan, G., and Soni, A.H., "Nonlinear Modeling of Kinematic and Flexibility Effects in Manipulator Design," ASME *J. of Mechanisms, Transmissions, and Automation in Design*, 110, Sept. 1988, pp. 243–254.

5 Wehage, R.A., and Shabana, A.A. "Application of Generalized Newton-Euler Equations and Recursive Projection Methods to Dynamics of Deformable

Multibody Systems," *Proc. 1989 ASME Design Technical Conferences—15th Design Automation Conference*, Montreal, Vol. 19-3, Sept. 1989, pp. 17–25.

6 Hughes, P.C., and Sincarsin, G.B., "Dynamics of Elastic Multibody Chains: Part B—Global Dynamics," *Dynamics and Stability of Systems*, Vol. 4, 3 and 4, 1989, pp. 227–243.

7 Nagarajan, S. and Turcic, D.A., "Lagrangian Formulation of the Equations of Motion for Elastic Mechanisms With Mutual Dependence Between Rigid Body and Elastic Motions. Part II: System Equations," ASME JOURNAL OF DYNAMIC SYSTEMS, MEASUREMENT, AND CONTROL. Vol. 112, June 1990, pp. 215–224.

8 D'Eleuterio, G.M.T., "Dynamics of Elastic Multibody Chains: Part C—Recursive Dynamics," *Dynamics and Stability of Systems*, Vol. 7, 2, 1992, pp. 61–90.

9 Kane, T.R., Ryan, R.R., and Banerjee, A.K. "Dynamics of a Cantilever Beam Attached to a Moving Base," *J. Guidance, Control, and Dynamics*, Vol. 10, 2, 1987, pp. 139–151.

10 Simo, J.C., and Vu-Quoc, L., "The Role of Non-linear Theories in Transient Dynamic Analysis of Flexible Structures," ASME *Journal of Sound and Vibration*, Vol. 119, 3, 1987, pp. 487–508.

11 Simo, J.C., and Vu-Quoc, L. "On the Dynamics of Flexible Beams under Large Overall Motions—The Plane Case: Part I," ASME *Journal of Applied Mechanics*, Vol. 53, 4, 1986, pp. 849–854.

12 Likins, P.W., Barbera, F.J., and Baddeley, V., "Mathematical Modeling of Spinning Elastic Bodies for Modal Analysis," *AIAA Journal*, Vol. 11, 1973, pp. 1251–1258.

13 Vigneron, F.R., "Comment on 'Mathematical Modeling of Spinning Elastic Bodies for Modal Analysis'," *AIAA Journal*, Vol. 13, 1975, pp. 126–127.

14 Kaza, K.R., and Kvaternik, R.G. "Nonlinear Flap-Lag-Axial Equations of a Rotating Beam," *Atca Astronautica*, Vol. 15, 6, 1977, pp. 1349–1360.

15 Lips, K.W., and Modi, V.J., "General Dynamics of a Large Class of Flexible Satellite Systems," *Acta Astronautica*, Vol. 7, 1980, pp. 1349–1360.

16 Hughes, P.C., and Fung, J.C. "Lyapunov Stability of Spinning Satellites with Long Flexible Appendages," *J. of Celestial Mechanics*, Vol. 4, 1971, pp. 295–308.

17 Vu-Quoc, L., and Simo, J.C. "Dynamics of Earth-Orbiting Flexible Satellites with Multibody Component," *J. Guidance, Control, and Dynamics*, Vol. 10, 6, 1987, pp. 549–558.

18 Banerjee, A.K., and Lemak, J.M. "Multi-Flexible Body Dynamics Capturing Motion-Induced Stiffness," ASME *Journal Applied Mechanics*, Vol. 58, 1991, pp. 766–775.

19 Walrapp, O., "Linearized Flexible Multibody Dynamics Including Geometric Stiffening Effects," *Mechanics of Structures and Machines*, Vol. 19, 3, 1991, pp. 385–409.

20 Padilla, C. E., and von Flotow, A. H., "Nonlinear Strain-Displacement Relations and Flexible Multibody Dynamics," *J. Guidance, Control, and Dynamics*, Vol. 15, 1, 1992, pp. 128–136.

21 Ider, S.K., and Amirouche, F.M.L., "Nonlinear Modeling of Flexible Multibody Systems Dynamics Subjected to Variable Constraints," ASME *Journal Applied Mechanics*, Vol. 56, 1989, pp. 444–450.

22 Van Woerkom, P.Th.L.M., "Modified Dynamics Modelling for Maneuvering Flexible Space Manipulators," *42nd Congress of the International Astronautical Federation*, IAF-91-356, Oct. 1991, Montreal.

23 Shabana, A.A., "Constrained Motion of Deformable Bodies," *International Journal for Numerical Methods in Engineering*, Vol. 32, 1991. pp. 1813–1831.

24 Sharf, I., and Damaren, C. J., "Simulation of Flexible-Link Manipulators: Basis Functions and Nonlinear Terms in the Motion Equations," *Proc. 1992 IEEE Conference on Robotics and Automation*, Nice, France, May, 1992, pp. 1956–1962.

25 Mayo, J., and Dominguez, J., "Geometrically Nonlinear Coupling Between Axial and Flexural Modes of Deformation of Multibody Systems," *Proc. 1992 ASME Winter Annual Meeting*, AMD-Vol. 141/DSC-Vol. 37, Anaheim, CA, 1992, pp. 95–106.

26 Meirovitch, L., "Hybrid State Equations of Motion for Flexible Bodies in Terms of Quasi-Coordinates," *J. Guidance, Control, and Dynamics*, Vol. 14, 5, 1991, pp. 1008–1013.

27 Simo, J.C., and Vu-Quoc, L., "On the Dynamics in Space of Rods Undergoing Large Motions—A Geometrically Exact Approach," *Computer Methods in Applied Mechanics and Engineering*, Vol. 66, 1988, pp. 125–161.

28 Cardona, A., and Geradin, M., "A Beam Finite Element Non-linear Theory with Finite Rotations," *International Journal for Numerical Methods in Engineering*, Vol. 26, 1988, pp. 2406–2438.

29 D'Eleuterio, G.M.T., "Notes on Nonlinearities in Flexible-Body Motion Equations," 1987.

30 Sincarsin, G.B., and Hughes, P.C., "Dynamics of Elastic Multibody Chains: Part A—Body Motion Equations," *Dynamics and Stability of Systems*, Vol. 4, 3 and 4, 1990, pp. 209–226.

31 Spencer, A.J.M., *Continuum Mechanics*, Longman, London, 1980.

32 D'Eleuterio, G. M. T., "Multibody Dynamics for Space Station Manipulators: Recursive Dynamics of Topological Chains," Dynacon Report SS-3, 1985.

33 Simo, J.C., and Vu-Quoc, L., "On the Dynamics of Flexible Beams under Large Overall Motions—The Plane Case: Part II," ASME *Journal of Applied Mechanics*, Vol. 53, 4, 1986, pp. 855–863.

34 Damaren, C.J. and D'Eleuterio, G.M.T. "On the Relationship Between Discrete-Time Optimal Control and Elastic Multibody Dynamics" *Contemporary Mathematics: Dynamics and Control of Multibody Systems*, Vol. 97, American Mathematical Society, Providence, RI, 1989.

35 Inman, D. J., *Vibration with Control, Measurement, and Stability*, Prentice Hall, Englewood Cliffs, NJ, 1989.

36 Wu, H. T., Mani, N. K., and Ashrafioun, H. "Modeling of Flexible Bodies for Dynamic Analysis of Mechanical Systems," *Proc. of the 1st National Applied Mechanisms and Robotics Conference*, Cincinnati, OH, Nov. 1989.

37 Przemieniecki, J. S., *Theory of Matrix Structural Analysis*, McGraw-Hill New York, 1968.

38 Hanagud, S., and Sarkar, S. "Problem of the Dynamics of a Cantilevered Beam Attached to a Moving Base," *J. Guidance, Control, and Dynamics*, Vol. 12, 3, 1989, pp. 438–441.